

# ChemComm

Chemical Communications

Accepted Manuscript

This article can be cited before page numbers have been issued, to do this please use: S. Gu, D. Li, D. Long, X. Yu, W. Li, S. Ma and P. Tao, *Chem. Commun.*, 2026, DOI: 10.1039/D6CC01319H.



This is an Accepted Manuscript, which has been through the Royal Society of Chemistry peer review process and has been accepted for publication.

Accepted Manuscripts are published online shortly after acceptance, before technical editing, formatting and proof reading. Using this free service, authors can make their results available to the community, in citable form, before we publish the edited article. We will replace this Accepted Manuscript with the edited and formatted Advance Article as soon as it is available.

You can find more information about Accepted Manuscripts in the [Information for Authors](#).

Please note that technical editing may introduce minor changes to the text and/or graphics, which may alter content. The journal's standard [Terms & Conditions](#) and the [Ethical guidelines](#) still apply. In no event shall the Royal Society of Chemistry be held responsible for any errors or omissions in this Accepted Manuscript or any consequences arising from the use of any information it contains.

## Unlocking efficient near-infrared circularly polarized phosphorescence reaching 800 nm via rational molecular engineering of cyclometalated Pt(II) complexes†

 Shilin Gu,<sup>a</sup> Dongsheng Li,<sup>a</sup> Deng Long,<sup>a</sup> Xinglin Yu,<sup>a</sup> Wentao Li,<sup>\*a</sup> Sihan Ma,<sup>\*a</sup> and Peng Tao<sup>\*b</sup>

 Received 00th January 20xx,  
Accepted 00th January 20xx

DOI: 10.1039/x0xx00000x

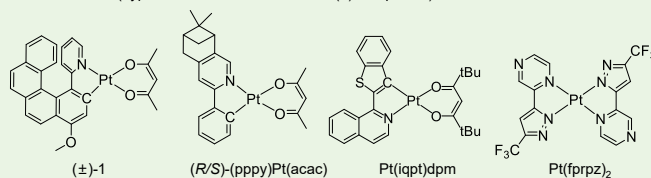
[www.rsc.org/](http://www.rsc.org/)

Achieving efficient near-infrared (NIR) circularly polarized phosphorescence (CPP) remains challenging. We report a promising strategy to design efficient NIR chiral Pt(II) complexes via ligand regulation and planar chirality formation. The point chirality of the bridging ligand enables exceptional diastereoselectivity promoted by the intramolecular Pt-Pt interaction, affording pure binuclear Pt(II) enantiomers that exhibit unprecedented NIR CPP reaching 800 nm, photoluminescence quantum yields of up to 35.4%, short lifetimes within 2  $\mu$ s, and luminescence dissymmetry factors of  $\sim 3.9 \times 10^{-3}$ .

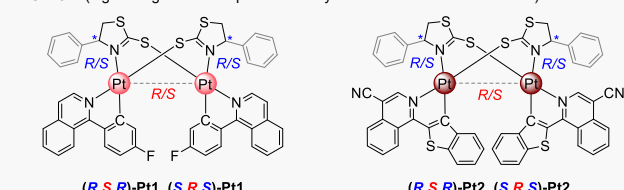
Near-infrared (NIR) circularly polarized (CP) luminescent (CPL) materials are promising for use in both biomedical engineering and optoelectronics.<sup>1</sup> Traditional methods of generating CP light via polarizers are energy-intensive.<sup>1</sup> Developing chiral luminescent materials that directly emit NIR CPL light is crucial. Integrating chirality into high-efficiency NIR emitters is therefore key to creating direct NIR CPL light sources with minimal energy loss. Phosphorescent transition-metal complexes (PTMCs) are particularly attractive because strong spin-orbit coupling (SOC) enables full utilization of both singlet and triplet excitons,<sup>2</sup> resulting in near-unity internal quantum efficiency.<sup>3</sup> Among PTMCs, the Pt(II) complexes are promising candidates owing to the easy realization of long-wavelength emission.<sup>2,3</sup> However, the traditional HC<sup>N</sup> ligand-based Pt(II) complexes usually suffered from the low photoluminescence (PL) quantum yields (PLQYs) in NIR region due to the lack of strong intermolecular interactions, leading to inefficient intersystem crossing (ISC) from the singlet excited state ( $S_1$ ) to the triplet excited state ( $T_1$ ).<sup>4</sup> Achieving Pt(II) complexes with high-efficiency near-infrared circularly polarized phosphorescence (CPP) remains a formidable challenge.<sup>1</sup>

The Pt-Pt interactions could promote the overlap of metal-centred orbitals, resulting in the formation of a low-energy triplet metal-metal-to-ligand charge transfer (<sup>3</sup>MMLCT) state, which typically serves as an energy trap.<sup>3c,5</sup> The enhanced metal character strengthens SOC, facilitating both ISC from  $S_1$  to  $T_1$  and formally forbidden triplet-to-singlet radiative transition, thereby increasing the radiative decay rate.<sup>5</sup> Meanwhile, the ordered molecular alignment induced by Pt-Pt interactions restricts ligand vibrations and rotations, effectively suppressing non-radiative decay pathways linked to molecular motion and significantly lowering the non-radiative decay rate.<sup>5</sup> Thus, engineering Pt-Pt interactions offers a promising strategy to reduce non-radiative loss in low-energy NIR Pt(II) emitters by enhancing the radiative decay rate

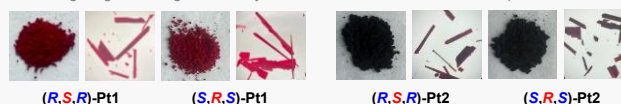
### Previous Work (Typical chiral or NIR emissive Pt(II) complexes)



### This Work (Ligand regulation and planar chirality formation via Pt-Pt interaction)



- ✓ Exceptional diastereoselectivity
- ✓ Intramolecular Pt-Pt interaction
- ✓ Planar and point chirality
- ✓ Long-range helix alignment in crystal
- ✓ NIR phosphorescence reaching 800 nm
- ✓ Circularly polarized phosphorescence
- ✓ High PLQYs of up to 35.4%
- ✓ Short lifetimes within 2  $\mu$ s



**Scheme 1.** Molecular engineering of cyclometalated Pt(II) complexes showing highly efficient NIR CPP reaching 800 nm in this work and the typical examples of the reported chiral or NIR emissive Pt(II) complexes. Insets show the photographs of these complexes in powder (left) and crystal (right) states under room light.

<sup>a</sup> Institute of Advanced Optoelectronic Materials and Technology, College of Big Data and Information Engineering, Guizhou University, Guiyang 550025, P. R. China. E-mails: wtl@gzu.edu.cn (W. Li); shma@gzu.edu.cn (S. Ma)

<sup>b</sup> Department of Applied Biology and Chemical Technology, The Hong Kong Polytechnic University, Hung Hom, Hong Kong, P. R. China; The Hong Kong Polytechnic University Shenzhen Research Institute, Shenzhen 518057, P. R. China. E-mail: pengtao@polyu.edu.hk (P. Tao)

† Electronic Supplementary Information (ESI) available: Synthesis, characterization, CCDC deposition numbers and other data. See DOI: 10.1039/x0xx00000x



constant and ultimately improving their PLQYs. Furthermore, although the Pt(II) complexes can be endowed with CPP upon the introduction of helical or point chirality,<sup>6</sup> the intramolecular Pt-Pt interactions could also provide the opportunity to generate planar chirality for realizing the circularly polarized phosphorescence of Pt(II) complexes.<sup>5</sup>

In this communication, a promising strategy was proposed to design highly efficient NIR chiral Pt(II) complexes (**(R,S,R)-Pt1**, **(S,R,S)-Pt1**, **(R,S,R)-Pt2**, and **(S,R,S)-Pt2**) via rational ligand regulation and planar chirality formation (**Scheme 1**). Two isoquinoline derivatives (i.e., 1-(4-fluorophenyl)isoquinoline and 1-(benzo[*b*]thiophen-2-yl)isoquinoline-4-carbonitrile) with low triplet energy levels were selected as the cyclometalating ligands. The point chirality of the bridging ligand enables exceptional diastereoselectivity promoted by the intramolecular Pt-Pt interaction, affording pure binuclear Pt(II) enantiomers that exhibit unprecedented NIR CPP reaching 800 nm, notable PLQYs of up to 35.4%, short excited state lifetimes within 2  $\mu$ s, and appreciable luminescence dissymmetry factors ( $g_{\text{lum}}$ ) of up to  $\sim 3.9 \times 10^{-3}$ . To the best of our knowledge, this is the first example of highly efficient NIR chiral binuclear Pt(II) complexes with CPP maxima reaching 800 nm.<sup>1</sup>

The target Pt(II) complexes were obtained as the deep-red or dark maroon solids by heating chiral bridging ligand with Pt(II) intermediate [Pt(F-piq)(F-Hpiq)Cl] or [Pt(CN-iqbt)(CN-Hiqbt)Cl] in the presence of  $\text{K}_2\text{CO}_3$  at 80 °C in a sealed tube with  $\text{CH}_2\text{Cl}_2$  under an argon atmosphere (**Scheme S1**). Notably, in all coordination reactions, only one enantiomerically pure product could be isolated, indicating nearly perfect diastereoselectivity (close to 100%). This high selectivity is likely driven by the point chirality of the chiral bridging ligand, which is in good agreement with previously reported observations.<sup>5bc</sup> These Pt(II) enantiomers were well characterized by the nuclear magnetic resonance (NMR)

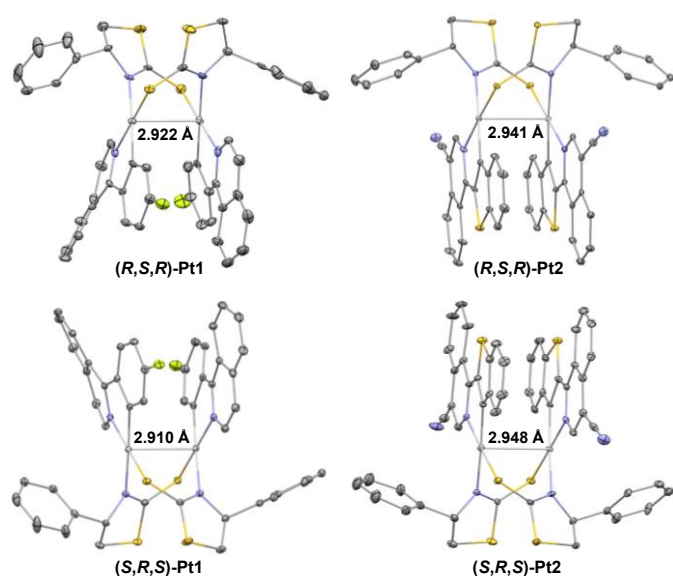


**Fig. 1** Crystal structures of the Pt(II) complexes showing the distance of the intramolecular Pt-Pt interactions. Note: The carbon atom is in gray, nitrogen atom is in light blue, platinum atom is in light gray, sulfur atom is in yellow, and fluorine atom is in yellow-green.

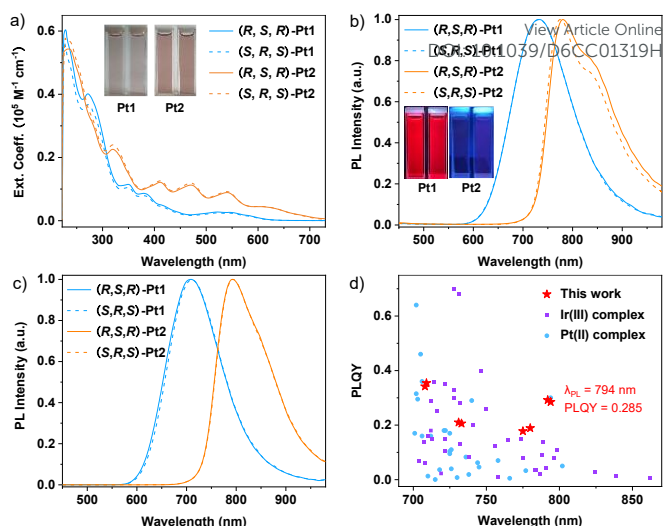


**Fig. 2** UV-vis absorption spectra (a) and PL spectra (b) of Pt(II) complexes in degassed  $\text{CH}_2\text{Cl}_2$ ; PL spectra (c) of Pt(II) complexes in 5 wt% PMMA film at room temperature; (d) comparison of PLQYs of designed Pt(II) complexes with the reported complexes showing PL at NIR region. Ext. Coeff. Refers to Extinction Coefficient.

spectroscopy, elemental analysis, and mass spectroscopy (MS).  $^1\text{H}$ ,  $^{13}\text{C}\{^1\text{H}\}$ , and  $^{19}\text{F}\{^1\text{H}\}$  NMR spectra all exhibit distinct and well-resolved resonance signals. The typical chemical shifts for the  $^1\text{H}$ ,  $^{13}\text{C}$ , and  $^{19}\text{F}$  nuclei are provided in **Tables S1**. For each pair of enantiomers, identical NMR spectra are observed in the  $\text{CDCl}_3$ , which is attributed to their identical atomic connectivity and equivalent electronic environments surrounding the nuclei. Only one  $^{19}\text{F}$  resonance signal ( $\sim 110.87$  ppm) was observed for **(R,S,R)-Pt1** and **(S,R,S)-Pt1**, implying the presence of the molecular symmetry in binuclear complexes.

The Pt(II) enantiomers were unambiguously confirmed by single-crystal X-ray diffraction analysis (**Table S2**). The crystallographic data revealed that the Pt(II) centres adopt a slightly distorted square-planar geometry. In this configuration, the nitrogen atoms from both the cyclometalated and bridging ligands are coordinated in a *trans* arrangement, while the metalated carbon and the sulfur atom from the adjacent bridging ligand are coordinated in a *cis* manner, which aligns with previously reported complexes.<sup>5,7</sup> The bond distances for Pt-C, Pt-N, and Pt-S fall within the ranges of 1.98–2.02 Å, 2.04–2.15 Å, and 2.28–2.30 Å, respectively (**Table S3**). Notably, the Pt-N bond lengths vary considerably depending on the N-donor strength of the ligands, with a significantly elongated Pt-N bond observed for the bridging ligand. Furthermore, the C-Pt-N bond angles are  $\sim 80^\circ$  (**Table S3**), indicating a minor deviation from ideal square-planar geometry, which can be attributed to the Jahn-Teller effect.<sup>5,7</sup> As shown in **Fig. 1**, short intramolecular Pt-Pt distances were observed, measuring 2.922 and 2.910 Å for **(R,S,R)/(S,R,S)-Pt1** enantiomers, and 2.941 and 2.948 Å for **(R,S,R)/(S,R,S)-Pt2** pair. The slightly longer Pt-Pt distances in the **Pt2** complexes compared to those in **Pt1** pair suggest that the intramolecular Pt-Pt interactions can be modulated by the choice of cyclometalating ligands. The two cyclometalated ligands are oriented in a head-to-tail manner. In all crystal structures, intermolecular face-to-face  $\pi$ - $\pi$  stacking interactions with distances ranging from 3.37 to 3.42 Å are observed between



partially overlapped cyclometalated ligands of adjacent molecules (Figs. S1 and S2, Table S4). Additionally, various weak intermolecular contacts including S...H and F...H interactions with separations below 3 Å are present throughout the crystals, contributing to the formation of a long-range helical arrangement (Fig. S3, Table S4).

To explore the optical properties of Pt(II) complexes, their ultraviolet (UV)-visible (vis) absorption spectra were measured in CH<sub>2</sub>Cl<sub>2</sub> at 1.0 × 10<sup>-5</sup> M at ambient temperature. As depicted in Fig. 2a, the complexes exhibit typical absorption profiles. An intense absorption band observed in the high-energy region (240–380 nm) originates from the π→π\* transitions of the ligands.<sup>5</sup> Conversely, the weaker and lower-energy absorption band spanning 380–700 nm is associated with MMLCT transitions (Table S5).<sup>5</sup> To gain deeper insight into the electronic transition characteristics, time-dependent density functional theory (TD-DFT) calculations were performed.<sup>8</sup> The simulated absorption profiles of the complexes in CH<sub>2</sub>Cl<sub>2</sub> are in good agreement with the experimental spectra (Fig. S4). The optimized S<sub>0</sub> and T<sub>1</sub> geometries of complexes and their Pt-Pt distances are shown in Fig. S5. For all Pt(II) complexes, the low-energy absorption bands predominantly arise from the transition between the highest occupied molecular orbital (HOMO) and the lowest unoccupied molecular orbital (LUMO), with a contribution exceeding 99% (Table S6). As depicted in Fig. 3, the HOMO electron density is mainly localized on the two Pt centres, whereas the LUMO is largely distributed across the cyclometalated ligands. This distribution further corroborates the assignment of the low-energy absorption to MMLCT transitions. As listed in Table S7, the Pt dπ orbital contributions to the HOMO and LUMO are 78.97% and 6.18% for (R,S,R)-Pt1, 79.10% and 6.00% for (S,R,S)-Pt1, 73.77% and 7.27% for (R,S,R)-Pt2, and 75.69% and 7.02% for (S,R,S)-Pt2, respectively. Meanwhile, the contributions from the π orbitals of the cyclometalated ligands to the HOMO and LUMO are 11.70% and 92.00% for (R,S,R)-Pt1, 11.39% and 92.25% for (S,R,S)-Pt1, 17.05% and 90.77% for (R,S,R)-Pt2, and 14.99% and 91.17% for (S,R,S)-Pt2, respectively. The TD-DFT-calculated HOMO-LUMO energy gaps are 2.99 and 2.94 eV for

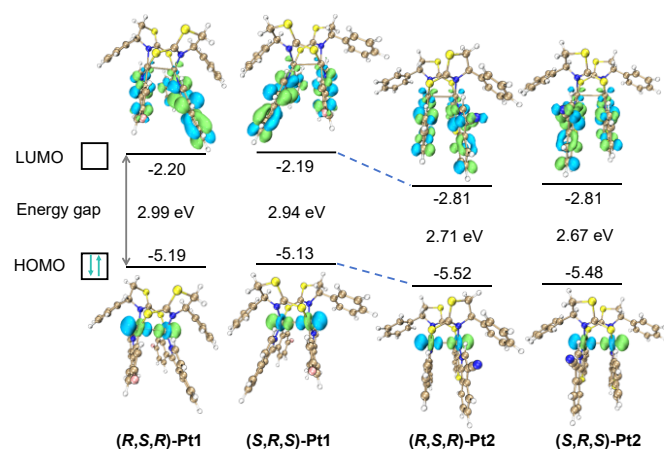


Fig. 3 Calculated electron cloud distributions and the orbital energy levels of LUMO and HOMO for Pt(II) complexes at their geometrical optimized ground state.

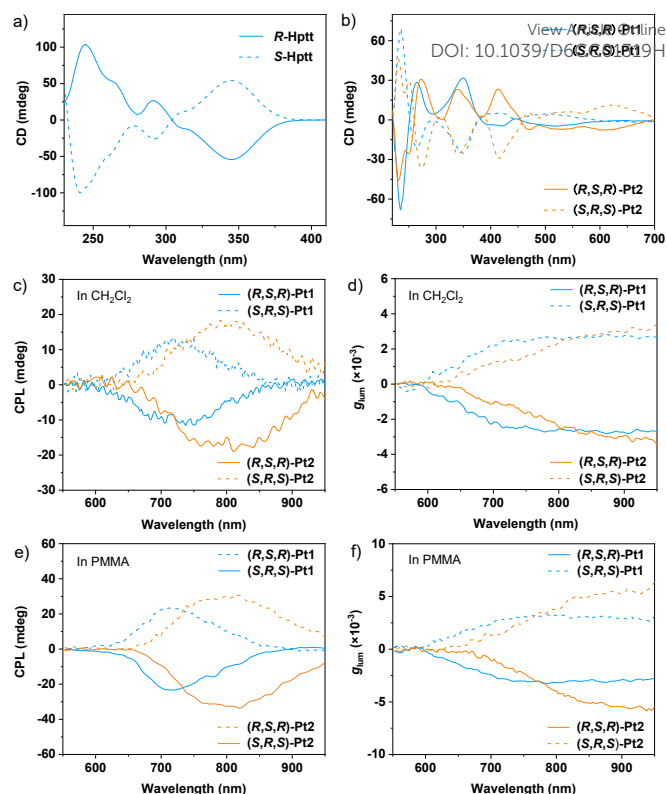


Fig. 4 CD spectra of free bridging ligands (a) and Pt(II) complexes (b) in CH<sub>2</sub>Cl<sub>2</sub>; The CPL (c,e) and  $g_{lum}$  profiles (d,f) of Pt(II) complexes in degassed CH<sub>2</sub>Cl<sub>2</sub> and PMMA film at room temperature.

the Pt1 enantiomers, and 2.71 and 2.67 eV for the Pt2 pair.

Upon UV light excitation, all Pt(II) enantiomers exhibit intense NIR phosphorescence both in degassed CH<sub>2</sub>Cl<sub>2</sub> and in poly(methyl methacrylate) (PMMA) films doped at 5 wt% under ambient conditions. As depicted in Fig. 2b and 2c, the Pt1 enantiomers show emission maxima at approximately 733 nm in degassed CH<sub>2</sub>Cl<sub>2</sub> and around 709 nm in the PMMA matrix. In contrast, the Pt2 pair display significantly red-shifted phosphorescence reaching 800 nm in both media, implying that the emission originates from individual molecules and the emission energies could be further decreased by lowering the triplet energy levels of cyclometalated ligands in the binuclear Pt(II) systems featuring strong intramolecular Pt-Pt interactions. Notably, the PLQYs of these complexes increase substantially upon dispersion in the rigid PMMA matrix, rising from 0.178–0.21 in degassed CH<sub>2</sub>Cl<sub>2</sub> to 0.285–0.354 in the doped films (Table S5). This enhancement indicates that non-radiative decay pathways are effectively suppressed in the rigid environment. Fig. 2d depicted the comparison of PLQYs of designed Pt(II) complexes in this work with the reported Ir(III) and Pt(II) complexes showing PL at NIR region, highlighting the effectiveness of the molecular design strategy employed in this work. The emission is further characterized by large Stokes shifts and long-lived excited states with lifetimes ranging from 0.32 to 0.40 μs in degassed CH<sub>2</sub>Cl<sub>2</sub> and 1.25 to 1.84 μs in PMMA films (Fig. S6, Table S5). These features are consistent with phosphorescence originating from triplet excited states.<sup>5</sup> The observed long-wavelength NIR



phosphorescence at room temperature can be ascribed to the intrinsically low triplet energy levels of the cyclometalated ligands, combined with the formation of triplet <sup>3</sup>MMLCT states facilitated by strong intramolecular Pt-Pt and π-π interactions.

The electrochemical behaviour of the Pt(II) complexes was investigated by cyclic voltammetry in CH<sub>3</sub>CN (Fig. S7). Oxidation potentials centred on the Pt atoms were determined to be 0.61/0.60 eV for the Pt1 enantiomers and 0.89/0.88 eV for the Pt2 pair (Table S8). This assignment is supported by DFT calculations, which reveal that the HOMO is predominantly localized on the Pt centers (Pt dπ orbital contributions: 73.77–79.10%), with minimal ligand contribution. From the absorption edges, the HOMO and LUMO energy levels were calculated to be –4.90/–4.89 eV and –2.93/–2.92 eV for Pt1 enantiomers, and –5.18/–5.17 eV and –3.58/–3.57 eV for Pt2 pair, respectively.

The chiroptical properties of the Pt(II) complexes were further evaluated in CH<sub>2</sub>Cl<sub>2</sub> using circular dichroism (CD) and CPL spectroscopy. As shown in Fig. 4, mirror-image CD signals were observed for each enantiomeric pair as well as for the corresponding free chiral ligands. The experimental CD spectra closely matched the simulated results (Fig. S8, Tables S9 and S10), further confirming the absolute configurations. Based on TD-DFT calculations, the CD bands in the 470–700 nm region primarily arise from planar chirality.<sup>7</sup> CPL spectra were acquired both in CH<sub>2</sub>Cl<sub>2</sub> solution and in PMMA films. Mirror-image CPL responses were clearly observed for each pair of enantiomers (Fig. 4c and 4e). The *g*<sub>lum</sub> at the emission maxima were determined to be –2.5/2.5 × 10<sup>–3</sup> in CH<sub>2</sub>Cl<sub>2</sub> and –2.8/2.7 × 10<sup>–3</sup> in PMMA for (R,S,R)/(S,R,S)-Pt1, and –2.1/2.1 × 10<sup>–3</sup> in CH<sub>2</sub>Cl<sub>2</sub> and –3.9/3.8 × 10<sup>–3</sup> in PMMA for (R,S,R)/(S,R,S)-Pt2 (Table S5, Figs. 4 and S9). As far as we know, this is the first example of NIR chiral binuclear Pt(II) complexes with CPP maxima reaching 800 nm.<sup>1</sup> For compounds with small molecular weight, *g*<sub>lum</sub> is given by  $g_{lum} = 4\cos\theta|\mu_e||\mu_m|/(|\mu_e|^2+|\mu_m|^2)$ , where  $\mu_e$  and  $\mu_m$  are the electric and magnetic transition dipole moments, and  $\theta$  is the angle between them.<sup>1</sup> The calculated  $|\mu_e|/|\mu_m|$  values (×10<sup>–20</sup>) are 3.9/0.006 for (R,S,R)-Pt1, 3.9/0.007 for (S,R,S)-Pt1, 2.9/0.002 for (R,S,R)-Pt2, and 3.0/0.002 for (S,R,S)-Pt2 (Table S10). The corresponding  $\theta$  values are 45.4°, 44.2°, 2.4°, and 0.4°, respectively. Notably, molecular structure exerts a much stronger influence on  $|\mu_m|$  and  $\theta$  than on  $|\mu_e|$ . As expected,  $|\mu_e|$  is substantially larger than  $|\mu_m|$  for all complexes. The simulated *g*<sub>lum</sub> values (3.3 × 10<sup>–3</sup> for (R,S,R)-Pt1, –3.4 × 10<sup>–3</sup> for (S,R,S)-Pt1, 1.8 × 10<sup>–3</sup> for (R,S,R)-Pt2, and –1.6 × 10<sup>–3</sup> for (S,R,S)-Pt2 are on the order of 10<sup>–3</sup>, consistent with typical values of reported analogues.<sup>1,9</sup>

To conclude, we have developed a series of chiral binuclear Pt(II) complexes achieving NIR CPP up to 800 nm through rational ligand regulation and planar chirality engineering. The intramolecular Pt-Pt interactions not only promote the formation of <sup>3</sup>MMLCT states but also facilitate planar chirality. These complexes exhibit notable PLQYs (up to 35.4%), short lifetimes (<2 μs), and appreciable *g*<sub>lum</sub> factors (~3.9 × 10<sup>–3</sup>), representing the first example of NIR CPL Pt(II) emitters reaching 800 nm. These results demonstrate that this design strategy will show great potential for developing high-performance NIR CPL emitters toward both biomedical and optoelectronic applications.

## Conflicts of interest

There are no conflicts to declare.

## Data availability

The data supporting this article have been included as part of the supplementary information (SI). Supplementary information is available. See DOI: <https://doi.org/10.1039/xxx>.

## Acknowledgements

We acknowledge the financial support from the Guizhou University Talent Program (X2023159), Guizhou Provincial Basic Research Program (Natural Science) (QKHJC MS[2025]606), Guizhou Provincial Basic Research Program (Natural Science-Youth Guidance) (QKHJC2024Y100), Youth Talent Growth Project of Guizhou Provincial Department of Education (QJJ2024023), Guangdong Basic and Applied Basic Research Foundation (2026A1515011199), Startup Fund for RAPs under the Strategic Hiring Scheme (P0035922).

## References

- 1 a) N. Liang, C. Cao, Z. Xie, J. Liu, Y. Feng and C.-J. Yao, *Mater. Today*, 2024, **75**, 309; b) X. Yang, X. Gao, Y.-X. Zheng, H. Kuang, C.-F. Chen, M. Liu, P. Duan and Z. Tang, *CCS Chem.*, 2023, **5**, 2760.
- 2 a) K. Y. Zhang, Q. Yu, H. Wei, S. Liu, Q. Zhao and W. Huang, *Chem. Rev.*, 2018, **118**, 1770; b) P. Tao, X. Lü, G. Zhou and W.-Y. Wong, *Acc. Mater. Res.*, 2022, **3**, 830; c) P. Tao and W.-Y. Wong, *Luminescent Transition-Metal Complexes and Their Applications in Electroluminescence*. In *Comprehensive Inorganic Chemistry III*, 3rd ed.; Elsevier: 2023; Vol. 8, pp 2–79; d) S. Hattori, K. Shinozaki, *ChemPhotoChem* 2025, **9**, e202500041.
- 3 a) P. Tao, J. Jin, X. Zheng, Y.-J. Pu and W.-Y. Wong, *Matter*, 2025, **8**, 102142; b) S. N. T. Phan, N. B. Nguyen and T. S. Teets, *Chem. Commun.*, 2025, **61**, 17544; c) K.T. Ly, R.-W. Chen-Cheng, H.-W. Lin, Y.-J. Shiau, S.-H. Liu, P.-T. Chou, C.-S. Tsao, Y.-C. Huang and Y. Chi, *Nat. Photonics*, 2017, **11**, 63; d) M. Wałęsa-Chorab, *J. Photochem. Photobiol. C Photochem. Rev.* 2024, **59**, 100664; e) H. J. Park, *Crystals* 2025, **15**, 273.
- 4 M. Penconi, M. Cazzaniga, S. Kesarkar, P. R. Mussini, D. Ceresoli and A. Bossi, *Photochem. Photobiol. Sci.*, 2017, **16**, 1220.
- 5 a) M. Yoshida and M. Kato, *Coord. Chem. Rev.*, 2018, **355**, 101; b) J. Song, H. Xiao, B. Zhang, L. Qu, X. Zhou, P. Hu, Z.-X. Xu and H. Xiang, *Angew. Chem. Int. Ed.*, 2023, **62**, e202302011; c) J. Song, H. Xiao, L. Fang, L. Qu, X. Zhou, Z.-X. Xu, C. Yang and H. Xiang, *J. Am. Chem. Soc.*, 2022, **144**, 2233.
- 6 a) J. R. Brandt, X. Wang, Y. Yang, A. J. Campbell and M. J. Fuchter, *J. Am. Chem. Soc.*, 2016, **138**, 9743; b) G.-Z. Lu, N. Su, Y. Li and Y.-X. Zheng, *J. Organomet. Chem.*, 2017, **842**, 39.
- 7 a) B. Zhang, Q. Yang, B. Tu, W. Dong, X. Zhou, J. Song and H. Xiang, *Org. Lett.*, 2025, **27**, 6971; b) S. Gu, D. Li, D. Long, X. Yu, S. Ma, W. Li, J. Liu, P. Tao and W.-Y. Wong, *Inorg. Chem.*, 2025, **64**, 22513.
- 8 M. J. Frisch, G. W. Trucks, H. B. Schlegel, G. E. Scuseria, M. A. Robb, J. R. Cheeseman, G. Scalmani, V. Barone, G. A. Petersson, H. Nakatsuji, X. Li, M. Caricato, A. V. Marenich, J. Bloino, B. G. Janesko, R. Gomperts, B. Mennucci, H. P. Hratchian, J. V. Ortiz, A. F. Izmaylov, J. L. Sonnenberg, D. Williams-Young, F. Ding, F. Lipparini, F. Egidi, J. Goings, B. Peng, A. Petrone, T. Henderson, D. Ranasinghe, V. G.



Zakrzewski, J. Gao, N. Rega, G. Zheng, W. Liang, M. Hada, M. Ehara, K. Toyota, R. Fukuda, J. Hasegawa, M. Ishida, T. Nakajima, Y. Honda, O. Kitao, H. Nakai, T. Vreven, K. Throssell, J. A., Jr. Montgomery, J. E. Peralta, F. Ogliaro, M. J. Bearpark, J. J. Heyd, E. N. Brothers, K. N. Kudin, V. N. Staroverov, T. A. Keith, R. Kobayashi, J. Normand, K. Raghavachari, A. P. Rendell, J. C. Burant, S. S. Iyengar, J. Tomasi, M. Cossi, J. M. Millam, M. Klene, C. Adamo, R. Cammi, J. W. Ochterski, R. L. Martin, K. Morokuma, O. Farkas, J. B. Foresman and D. J. Fox, Gaussian 16, Revision C.01, Gaussian, Inc., Wallingford, CT, 201.

- 9 a) J. Han, S. Guo, H. Lu, S. Liu, Q. Zhao and W. Huang, *Adv. Opt. Mater.*, 2018, **6**, 1800538; b) H. Lu, L. Di Bari, L. and Favereau, *Nat. Photonics*, 2025, **19**, 1041; c) F. J. Coughlin, M. S. Westrol, K. D. Oylar, N. Byrne, C. Kraml, E. Zysman-Colman, M. S. Lowry and S. Bernhard, *Inorg. Chem.*, 2008, **47**, 2039; d) Y. Deng, M. Wang, Y. Zhuang, S. Liu, W. Huang and Q. Zhao, *Light Sci. Appl.*, 2021, **10**, 76.

View Article Online  
DOI: 10.1039/D6CC01319H



### Data availability

The data supporting this article have been included as part of the supplementary information (SI). Supplementary information is available. See DOI: <https://doi.org/10.1039/xxx>.

